Controllable Synthesis of Polynuclear Metal Clusters Within Macrocycles

43

Siqi Zhang and Liang Zhao

Contents

43.1 Introduction

The history of macrocyclic complexes dates back a long time to the biologically occurring macrocycles such as porphyrins and corrins, which function to bind metal ions at the active sites in a variety of nature systems (e.g., hemoglobin, cytochrome C, and vitamin B_{12}) [1, 2]. These natural macrocycles are taken as models in the early synthetic macrocyclic chemistry and give rise to an evolution of mimicking the metal-macrocycle active centers in biological systems. During the last few decades, significant progresses have been made in organic synthetic chemistry; thus a variety of macrocycles with internal anionic moieties such as -OH groups or neutral ones have been successfully fabricated [3–5] and applied in recognizing metal ions as

S. Zhang · L. Zhao (✉)
Key Laboratory of Bioorganic Phosphorus Chemistry and Chemical Biology (Ministry of Education), Department of Chemistry, Tsinghua University, Beijing, China
e-mail: Si_Qi_zhang@163.com; zhaolchem@mail.tsinghua.edu.cn

Y. Liu et al. (eds.), *Handbook of Macrocyclic Supramolecular Assembly*,
https://doi.org/10.1007/978-981-15-2686-2_49

well as stabilizing short-lived reactive species [6–8]. Such remarkable stability of these metal-macrocycle complexes comes from the known macrocyclic effect [9], which often brings about an enhanced kinetic and thermodynamic stability for the macrocycle systems compared with their open-chain analogues, thus making them ideal for mimicking the active sites of metalloenzymes in nature. By virtue of these outstanding properties of macrocyclic ligands, it is envisioned that the employment of macrocycles may provide a feasible method to achieve highly active models for metallobiosites in a convenient way.

Recent studies in the field of metal-macrocycle complexes synthesis have illustrated that the size-tunable macrocyclic ligands possess a good prospect in adjusting the nuclearity number of the resulting metal ion species based on size-match principle [10]. Therefore, we anticipate that the characteristic flexible conformations of large macrocyclic ligands would make them easily adapt to diversiform metal cluster aggregates, which play a significant role in mimicking the active sites of metalloenzymes on account of their fantastic properties. Since the structure diversities in nuclearity number and geometry largely affect the properties of metal cluster aggregates, it is essential to develop an efficient synthetic approach toward the controllable synthesis of metal clusters for further studies of their properties and applications. In this chapter, special attention is paid to the controllable synthesis of metal clusters based on macrocyclic template. Accordingly, reactivity studies and applications of the metal-macrocycle species are also exemplified.

43.2 Macrocyclic Ligands in Metal Cluster Synthesis

Polynuclear metal clusters have attracted intense interests of chemists in many interdisciplinary areas of chemistry owing to their fantastic catalytic properties, especially for mimicking the active sites of metalloenzymes which are ubiquitous in nature [11–14]. For instance, the widely studied copper-containing enzymes such as multicopper oxidases (MCOs) [15] and particulate methane monooxygenase (pMMO) [16] have exhibited efficient catalytic reactivities in the oxidation of phenol or methane. The active sites in these species are proposed to be polynuclear copper clusters. Thus, the designed synthesis of metal clusters with structural diversity plays an important role in studying the fundamental chemistry of enzyme-catalyzed reactions and developing new catalysts. Apart from the high reactivity empowered by their unique structures, however, the formidable structural complexity makes the rational design and controllable synthesis of polynuclear metal clusters very challenging. In this regard, the employment of structurally well-defined macrocyclic ligands has many advantages. Macrocyclic ligands could not only facilitate the formation of unique architectures based on their multiple coordination sites but also largely enhance their affinity for metal ions and form metal clusters with high kinetic inertness and thermodynamic stability due to the macrocyclic effect. Aside from this, the great advances in organic synthetic chemistry make it feasible to design and synthesize various desired macrocyclic compounds [17–19]. Recent studies in the field of metal-macrocycle complexes synthesis have illustrated that

the restricted conformational flexibility associated with the size-tunable macrocyclic ligands possess a good perspective in matching the cavity size of the macrocycle to the steric and electronic requirements of the resulting metal cluster species based on the size-match principle. Several metal cluster-macrocycle systems and single metal coordination complexes of oversized macrocycles are summarized below based on the classifications of coordination donor atoms within macrocycles.

43.2.1 Sulfur-Containing Macrocycles

Sulfur-containing macrocycles (thiamacrocycles) have been widely studied and often shown unusual coordination behavior toward soft metal ions such as Ag(I) and Cu(I) due to their well-documented affinity for soft sulfur donors, giving rise to a variety of supramolecular complexes with structural diversity. Besides, the latter d-block elements that are free of crystal field influences could readily adopt variable coordination numbers or geometries, which is conducive to the construction of uncommon structures. Molecular structures of several characteristic sulfur-containing macrocycles related to the synthesis of polymetallic species are presented here (Fig. 1).

Structure identification of blue copper proteins such as plastocyanin, azurin, and rusticyanin has illustrated that thiaether moieties play an important role as the coordination ligands to the copper centers. The construction of S-coordinated copper species as models of the active sites in "blue" copper proteins offers an efficient way to study the relationship between the coordination geometry and the redox behavior of the copper ions. To date, a number of sulfur-containing macrocycles have been applied to the study of copper species. For example, the S_6-donor ligand **[21]aneS$_6$** has been successfully employed to investigate the active sites of the "blue" copper proteins [20]. It is intriguing that the Cu(I) complex is found to be more stable than the Cu(II) complex by 12 orders of magnitude in the stability constant, which is probably attributed to the favor of tetrahedral geometry for copper(I) ions within this large flexible macrocycle. The structure of Cu(I) complex **1** (Fig. 2) shows that four adjacent sulfur donor atoms of **[21]aneS$_6$** participate in the coordination to the Cu(I) ion, giving a common distorted tetrahedral coordination geometry. The remaining two sulfur atoms in the ligand are free of coordination. Cyclic voltammetry measurement has revealed that the redox potential of the Cu(I)/Cu(II)couple in this system is 0.89 V (vs. SHE), which at the time is the highest reported value for a Cu(II/I) system in aqueous media.

An intriguing feature of thiamacrocycles is the ability to stabilize a variety of metal species with uncommon oxidation states. As in the following example, the first +2 oxidation-state silver complex [Ag**[18]aneS$_6$**]$^{2+}$ has been successfully isolated and characterized by using **[18]aneS$_6$** [21]. The single-crystal structure of [Ag**[18]aneS$_6$**]$(ClO_4)_2$ (**2**) confirms an octahedral homoleptic thioether coordination of the silver center with Ag(II)-S distances (2.569(7) Å and 2.720(6) Å) shorter than that in Ag(I) species (2.6665(12) Å and 2.7813(10) Å) (Fig. 3). Further DFT computations and EPR spectroscopy characterizations are performed to investigate the structure,

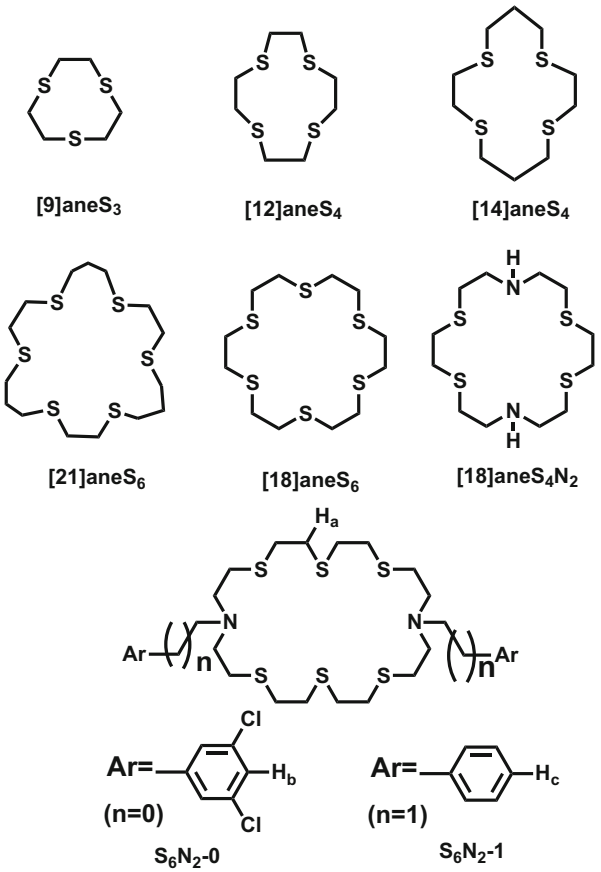

Fig. 1 Sulfur-containing macrocycles discussed in this chapter

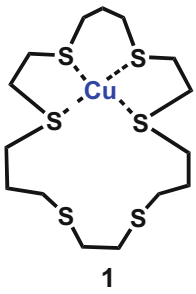

Fig. 2 The structure of Cu(I) complex encircled by **[21]aneS$_6$** macrocyclic ligand

which is in agreement with the XRD analysis. It is envisioned that the stereochemical flexibility of the crown ligands and their encapsulation of reactive metal ions by polarizabale S-donors are conducive to stabilize uncommon oxidation-state metal species.

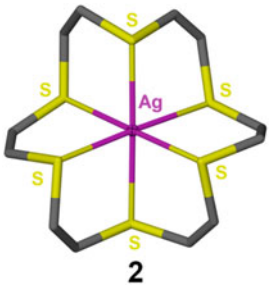

Fig. 3 Crystal structure of [Ag**[18]aneS$_6$**](ClO$_4$)$_2$ (**2**). Color coding: Ag, pink; C, gray; S, yellow

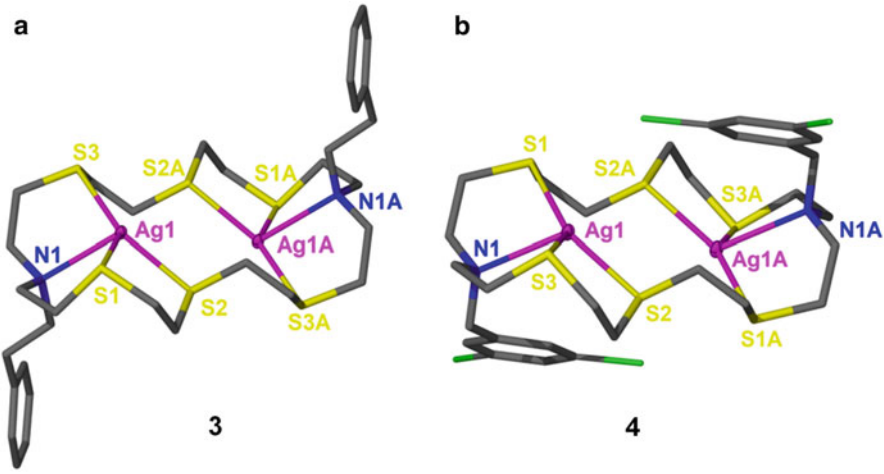

Fig. 4 Crystal structures of binuclear silver complexes **3** and **4** based on azathiacrown ethers. Color coding: Ag, pink; C, gray; N, blue; S, yellow; Cl, green

Many kinds of large azathiacrown ethers have also been prepared to encapsulate several Ag ions. An investigation on two azathiacrown ethers with N-appended side arms (**S$_6$N$_2$–0** and **S$_6$N$_2$–1**) shows that they both form 2:1 (metal/ligand) silver(I) complexes based on ^{1}H NMR titration and X-ray diffraction studies [22]. The structural studies of the binuclear silver complexes show that both Ag(I) ions are placed in the cavity of the macrocyclic ring and each silver(I) ion adopts a distorted trigonal bipyramidal geometry. Therein, three equatorial coordination sites and one axial position are taken up by three S atoms and one N atom from the macrocyclic ring, respectively (Fig. 4).

Aside from the group 11 metal complexes mentioned above, a series of cadmium (II) complexes containing differently sized thiamacrocyclic ligands have been reported. One goal of this study is to examine how structural modifications of thiamacrocycles affect their ability to bind toxic heavy metal ions [23]. Various Cd-macrocycle complexes of the thiamacrocyclic ligands illustrated in Fig. 1 have been successfully isolated. X-ray crystallographic structure of [Cd(**[9]aneS$_3$**)$_2$](PF$_6$)$_2$ (**5**) (Fig. 5a) shows that two **[9]aneS$_3$** ligands bind facially via their three sulfur atoms to a

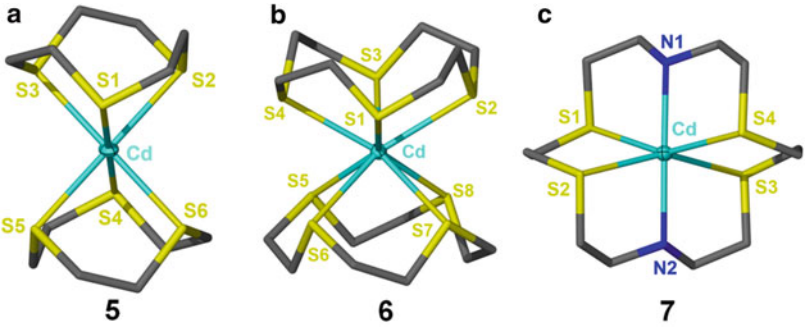

Fig. 5 Crystal structures of (**a**) [Cd(**[9]aneS$_3$**)$_2$](PF$_6$)$_2$ (**5**), (**b**) [Cd(**[12]aneS$_4$**)$_2$](ClO$_4$)$_2$ (**6**), and (**c**) [Cd**[18]aneS$_4$N$_2$**](PF$_6$)$_2$ (**7**). Color coding: Cd, light blue; N, blue; C, gray; S, yellow

Cd by a common distorted octahedral coordination geometry. As to an analogue complex [Cd(**[12]aneS$_4$**)$_2$](ClO$_4$)$_2$ (**6**) containing a larger thiamacrocycle **[12]aneS$_4$**, a sandwich-like structure is obtained as each **[12]aneS$_4$** binds the central Cd(II) ion via its four sulfur atoms to form an unusual eight-coordination square antiprismatic geometry (Fig. 5b). The Cd(II) complex **7** of the mixed azathiacrown **[18]aneS$_4$N$_2$** crystallized as a hexafluorophosphate salt (Fig. 5c). The coordination geometry of the Cd(II) center is found to be a severely distorted octahedral mode due to the mixed S/N donor system. The ^{113}Cd NMR chemical shifts of these Cd(II) complexes containing differently sized thiamacrocyclic ligands are in the range of 225 to 731 ppm. It is notable that the decrease in the number of thioether sulfur donors or the replacement of a thioether by a secondary nitrogen donor often causes upfield chemical shift in the ^{113}Cd NMR spectra. This finding provides a promising method for relating the ^{113}Cd NMR shift behaviors to the coordination environments in Cd(II) complexes involving thiamacrocyclic ligands.

Thiamacrocycles have also been widely applied to synthesize ruthenium(II) complexes. For example, the employment of differently sized thiamacrocycles **[9]aneS$_3$**, **[12]aneS$_4$**, and **[14]aneS$_4$** has led to [(Ru**[9]aneS$_3$**Cl)$_2$(bpta)](PF$_6$)$_2$ (**8**), [(Ru**[12]aneS$_4$**)$_2$(bpta)](PF$_6$)$_4$ (**9**), and [(Ru**[14]aneS$_4$**)$_2$bpta](PF$_6$)$_4$ (**10**) (bpta = 3,6-bis(2-pyridyl)-1,2,4,5-tetrazine) [24]. These complexes have a common bridged structure as shown in Fig. 6a–c. Various characterizations have been employed to probe the relationship between the electronic properties of bpta-bridged dinuclear Ru complexes and thioether ligands. X-ray crystallographic analysis of complex **8** has revealed that each Ru(II) ion is in a distorted octahedral coordination geometry and is coplanar with the bpta ligand. Three trans angles at the Ru(II) site (N-Ru-S, 176.56(15)° and 172.87(14)°; S-Ru-Cl, 175.20(6)°) have a slight variation away from the ideal octahedral coordination geometry. Compared with the relatively long bond lengths of Ru1-S1 and Ru2-S6, the shorter one of Ru1-S2 (2.3033(17) Å) results from the greater trans effect of chlorine. In complex **9** that contains a larger macrocycle **[12]aneS$_4$** with four sulfur donors, there is an obvious difference among three trans angles at the Ru(II) site (N-Ru-S, 177.96(18)° and 171.71(19)°; S-Ru-S, 176.34(8)°). These distortions are probably due to the increased steric hindrance of the large macrocycle, in which all

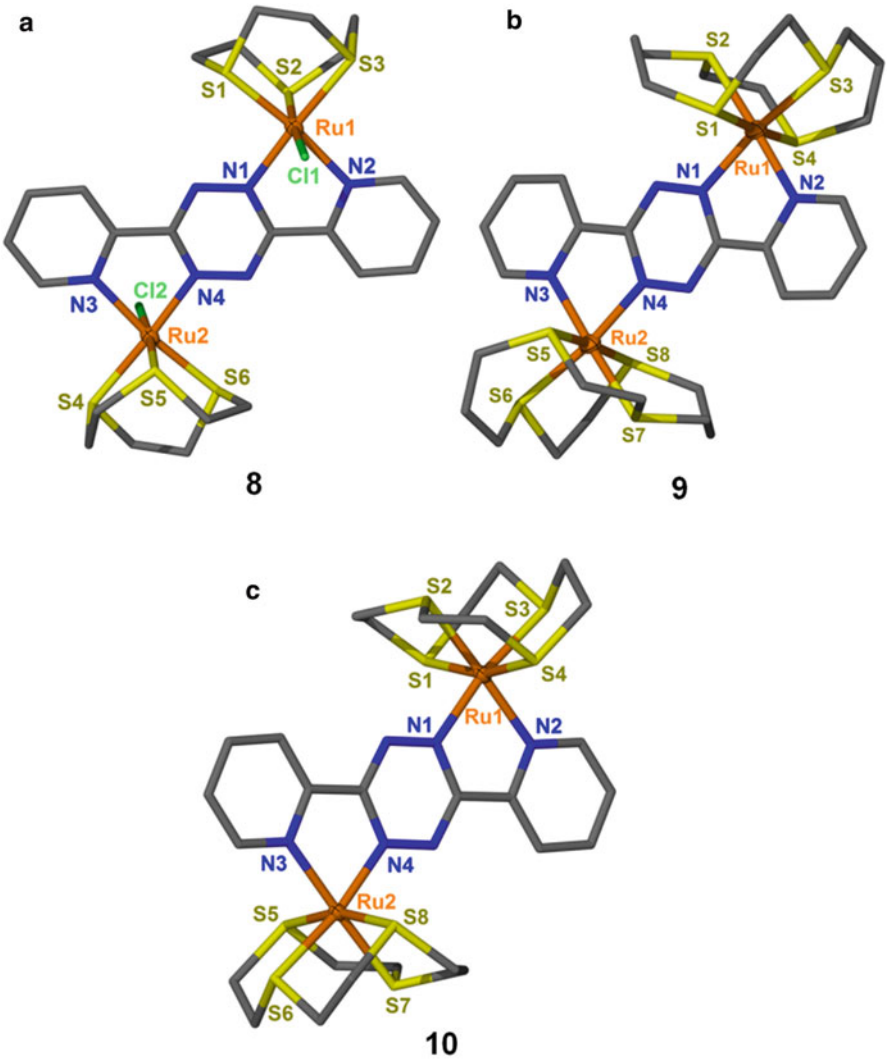

Fig. 6 Crystal structures of (**a**) $[(Ru\mathbf{[9]aneS_3}Cl)_2(bpta)](PF_6)_2$ (**8**) (**b**), $(Ru\mathbf{[12]aneS_4})_2(bpta)](PF_6)_4$ (**9**), and (**c**) $[(Ru\mathbf{[14]aneS_4})_2bpta](PF_6)_4$ (**10**). Color coding: Ru, orange; N, blue; C, gray; S, yellow; Cl, green

the four sulfur donor atoms are confined to a relatively small host cavity. The structure of complex **10** is very similar to that of **9** with each Ru(II) coordinated by four sulfur donor atoms. However, the larger and more flexible conformation of **[14]aneS$_4$** makes it better satisfy the octahedral coordination geometry. Furthermore, the UV-vis spectroscopy and electrochemical studies are then performed on these Ru complexes. Compared with chlorine-coordinated complex **8**, the significant changes for complexes **9** and **10** are the anodic shift of the bpta/bpta – couple and the $Ru^{III/II}$ couple, which may be related to the

bonding properties of thiacrown ligands. Due to the poor σ-donors but good π-acid characteristic of thioether ligands, the electron density on the Ru center in **8** would be decreased by introducing the chloride ligand. On the other hand, the decreased electron density could be achieved through increasing the backbonding to the thiacrowns, which then leads to a lowered intermetallic electronic coupling.

43.2.2 Oxygen Donor Macrocycle Systems

Macrocycles involving phenoxy bridges have been investigated for long time in supermolecular chemistry due to their persistent shape and a hydroxyl-based crown ether-like interior, which possess a great potential to coordinate with metal ions. A number of studies have demonstrated that oxygen-containing macrocycles could be used as scaffold to template the formation of various metal cluster aggregates. For example, some Zn(II) [25] or Cd(II) [26] acetate clusters could be obtained by using the phenoxy-based macrocyclic ligands. Single-crystal X-ray diffraction studies of **11** reveal that each zinc ion is supported by a N_2O_2 unit of the macrocycle, finally resulting in a distorted tetrahedral $[Zn_4O]$ cluster in cooperation with the bridged acetate ligands (Fig. 7a). Besides, this phenoxybased macrocyclic scaffold could also be applied to $Cd(OAc)_2$ H_2O system to obtain a heptacadmium carboxylate cluster (12). As shown in Fig. 7b, the macrocycle in **12** exhibits a bowl-shaped configuration to adapt to the formed Cd-oxygen cluster. Three Cd(II) ions each is coordinated by a N_2O_2 unit, and the remaining four central cadmium ions are coordinated by several oxygen atoms. This coordination scenario is analogous to the Zn(II) system. The ^{113}Cd NMR studies of **12** further confirm that the cadmium ions therein are located in three coordination environments with a ratio of 3:1:3, which is in agreement with the X-ray crystallographic structure. Moreover, the individual cluster-embedded bowls would corporate in pairs to form a capsule-like structure through hydrogen bonding, which is significantly influenced by different solvent systems.

In addition to the trap of homonuclear metal cluster species, such oxygen-containing macrocycles could also be applied to achieve heteronuclear cluster aggregates. One example is the macrocycle-involved tetranuclear mixed-metal complex **13**, which is composed of zinc and erbium ions in a 3:1 ratio [27]. Crystal structure of **13** indicates that both the tetradentate and hexadentate coordination modes are included in the macrocyclic ring. The former N_2O_2 is adopted by three Zn(II) ions, while the remaining Er(III) ion is joined by six phenoxy oxygen atoms of the macrocycle (Fig. 7c). In this way, the Er(III) ion is nine coordinated by six bridging oxygen atoms at equatorial positions and three oxygen atoms from a bidentate nitrato anion and water at the axial positions. The equatorial plane of the six phenoxy oxygen atoms is slightly bent with two oxygen atoms located above the ideal plane and the other four oxygen atoms below the plane. However, such deviations are neglectable in comparison with the remarkably different Er-O distances, which could be attributed to the strong equatorial ligand field of six phenoxy oxygen donors. The Zn(II) ions are in a square pyramidal coordination geometry

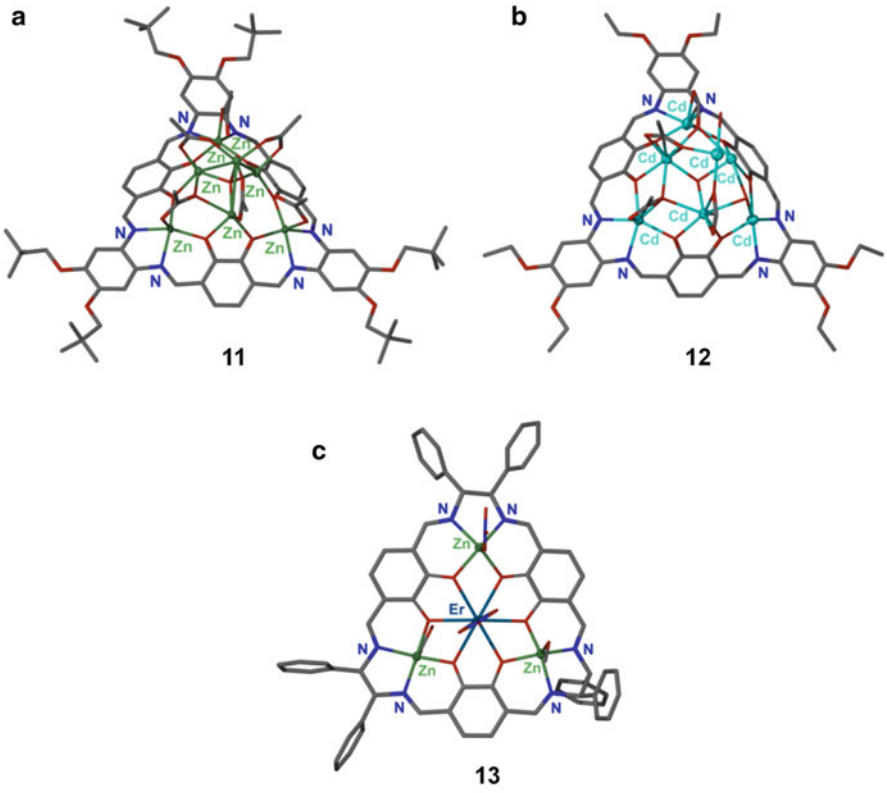

Fig. 7 Crystal structures of (**a**) $[Zn_4O(OAc)_6]$ (**11**), (**b**) $[Cd_3O(OAc)_6Cd(H_2O)_3]$ (**12**), and (**c**) $[Er^{III}Zn^{II}_3(OAc)(NO_3)_2(H_2O)_{1.5}(MeOH)_{0.5}]$ (**13**) clusters based on oxygen-containing macrocycles. Color coding: Zn, dark green; Cd, light blue; Er, dark blue; N, blue; C, gray; O, red

with a square N_2O_2 coordination site on the macrocyclic ligand and other molecules (acetate, nitrate, or methanol) at axial positions. In a short summary, macrocycles with pendant oxygen donors facilitate the formation of various homonuclear or heteronuclear metal cluster aggregates through the coordination and electrostatic attraction of bridging phenoxy oxygen atoms. Novel metal clusters with structure diversity have been achieved by this kind of macrocyclic templates.

43.2.3 Neutral N-Containing Macrocycle Systems

Aside from the widely utilized negatively charged macrocycles containing oxygen donors, neutral N-containing polydentate macrocycles have also been extensively employed in the assembly of metal cluster aggregates. Azacalix[*n*]pyridines (**Py[*n*]**s) [28] as a new kind of neutral macrocycles have been successfully applied in the

controllable synthesis of many anion-centered polynuclear metal clusters [10]. Taking advantage of the characteristic flexible conformation and tunable size of **Py[*n*]**s, they could easily adapt to structurally diversified metal cluster aggregates with different nuclearity numbers and coordination geometries. For example, a variety of **Py[*n*]**-based polynuclear silver clusters with many externally introduced mono-, di-, or multitopic anions (e.g., acetylides, thiolates, and halides) have been isolated and characterized [10]. It is noteworthy that the solubility of stoichiometric silver complexes of these anions is usually very poor (e.g., $K_{sp}(Ag_2S) = 8 \times 10^{-51}$ at 25 °C). However, the use of **Py[*n*]** macrocycles could largely enhance the solubility of related silver compounds due to the remarkable cooperative coordination effect.

For example, the polymeric silver acetylide complex $[AgC \equiv C^tBu]_n$ has poor solubility in common solvents. Nevertheless, treatment of a suspension of insoluble $[AgC \equiv C^tBu]_n$ and silver triflate with **Py[8]** leads to a clear pale-yellow solution immediately [29]. The crystallized product is subsequently obtained by the diffusion of diethyl ether into the solution. As shown in Fig. 8a, the formula of this crystalline complex **14** is revealed as $[(CF_3SO_3)Ag_4(^tBuC \equiv C)(\mathbf{Py[8]})](CF_3SO_3)_2$, which contains a square planar tetranuclear silver aggregate bridged by a $^tBuC \equiv C$ anion through σ and π interaction. Relative to the $^tBuC \equiv C$ anion, a triflate group is coordinated to an edge of the Ag_4 plane at the opposite side. Besides, the **Py[8]** macrocyclic ligand functions as an outer template to stabilize the Ag_4 aggregate based on the size-match principle. Notably, the linear $[(CF_3SO_3)Ag_4(^tBuC \equiv C)]$ moiety with the $^tBuC \equiv C$ anion and the triflate group bonded to the Ag_4 plane on either side is threaded through the **Py[8]** macrocycle, thus giving rise to a cluster-centered organometallic rotaxane structure. In contrast to the parallelogram 1,3,4,6-alternate conformation of free **Py[8]** macrocycle, the **Py[8]** in complex **14** is in a cylinder-belt-like conformation. It is intriguing that only one set of broad proton signals corresponding to the **Py[8]** ligand are observed in the ^1H NMR spectrum of **14** (Fig. 8b), which conflicts with its coordination behavior in the crystalline structure. In crystalline solid structure of **14**, two kinds of pyridine rings that are coordinated or uncoordinated with Ag can be clearly discriminated. Further variable temperature NMR studies show that the broad signals gradually split into several sharp doublets and triplets as the temperature decreases, suggesting that the **Py[8]** in **14** is fluxional in solution, and eight pyridyl nitrogen atoms undergo a rapid dissociation-recombination equilibrium to coordinate with the central Ag_4 aggregate.

Encouraged by the successful synthesis of the cluster-centered organometallic rotaxane **14**, a specific angled ditopic ligand is then applied to construct desired metal cluster-centered supramolecular architectures. As shown in Fig. 8c, the employment of the extending conjugated ligand 1,3-bis((3-ethynylphenyl)ethynyl) benzene affords two $[(C \equiv C)\text{-}Ag_4(CF_3SO_3)]$ aggregates at each anionic center, which is threaded through a **Py[8]** macrocycle to generate a pseudorotaxane structure in complex **15** [29]. In contrast to complex **14**, the two cluster-centered pseudorotaxane moieties constitute a semicircular [3]-pseudorotaxane structure based on the angled phenylene-acetylene linker. Furthermore, two semicircles are linked together by the F···F interactions between the attached triflates to finally yield a nanometer-sized hexagonal catenane-like structure (Fig. 8d).

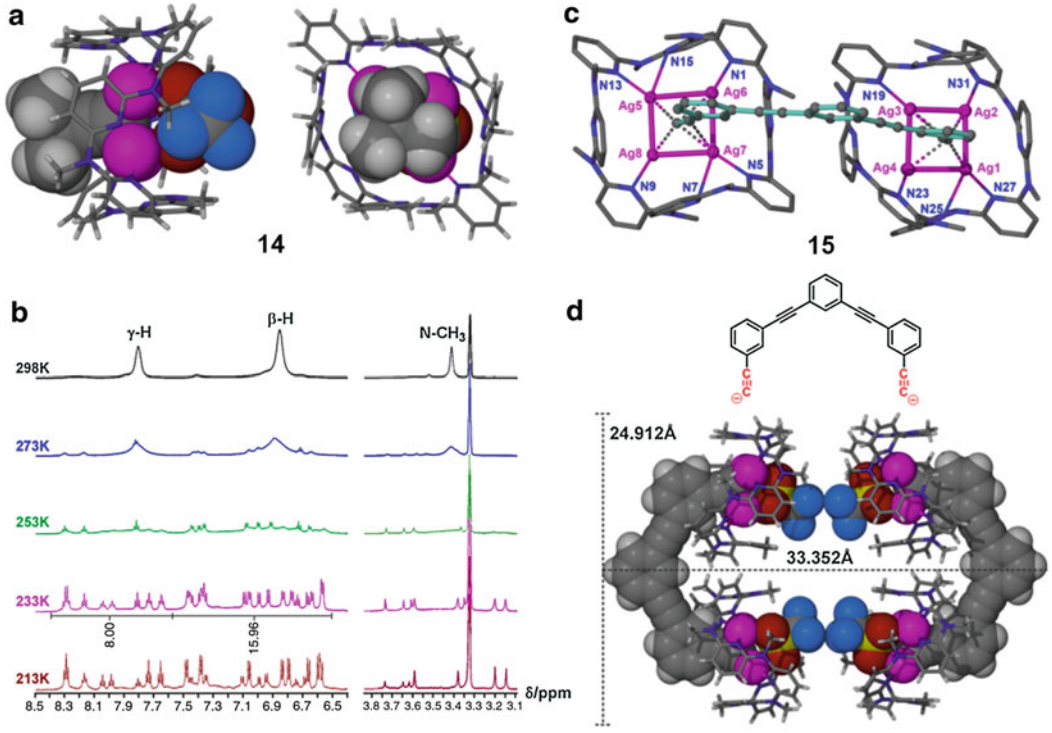

Fig. 8 (**a**) Crystal structure and (**b**) ^{1}H NMR of $[(CF_3SO_3)Ag_4(^{t}BuC \equiv C)(\mathbf{Py[8]})](CF_3SO_3)_2$ (**14**). (**c**) Crystal structure and (**d**) assembled hexagonal catenane-like structure of $[(CF_3SO_3)Ag_4\text{-}\{C \equiv C\text{-}(m\text{-}C_6H_4)\text{-}C \equiv C\text{-}(m\text{-}C_6H_4)\text{-}C \equiv C\text{-}(m\text{-}C_6\text{-}H_4)C \equiv C\}Ag_4(CF_3SO_3)(\mathbf{Py[8]})_2](CF_3SO_3)_4$ (**15**). Color coding: Ag, pink; N, blue; C, gray; O, red; the acetylide group is highlighted in green. (Reprinted with permission from [10, 29]. Copyright 2018 and 2011 American Chemical Society)

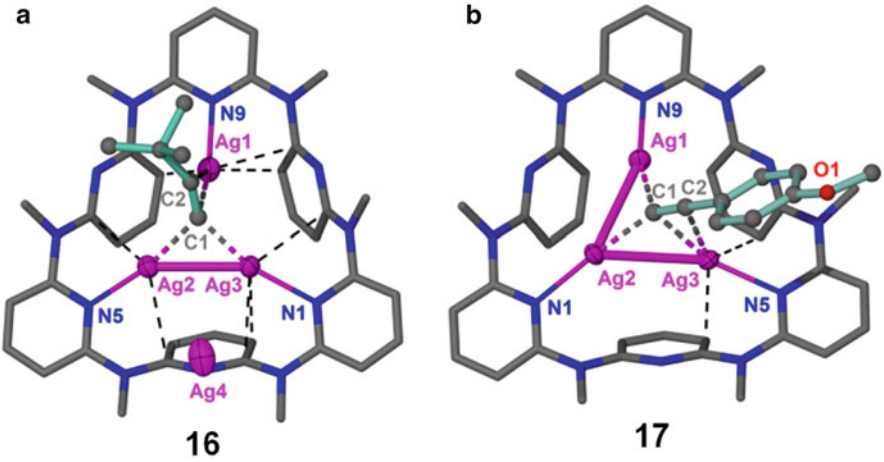

Fig. 9 Crystal structures of (**a**) $[(CF_3SO_3)_{1.5}Ag_{3.5}(^tBuC \equiv C)$(**Py[6]**)$-(CH_3OH)_{0.5}](CF_3SO_3)$ (**16**) and (**b**) $[Ag_3(p\text{-}MeOC_6H_4C \equiv C)$(**Py[6]**)$](CF_3SO_3)_2$ (**17**). Color coding: Ag, pink; N, blue; C, gray; O, red; the acetylide group is highlighted in green. (Reprinted with permission from [10]. Copyright 2018 American Chemical Society)

The size-tunable **Py[*n*]** macrocycles have a remarkable advantage in adjusting the nuclearity number of encapsulated polynuclear metal clusters. The employment of a smaller macrocycle **Py[6]** in place of **Py[8]** results in a trinuclear silver aggregate (**16** and **17**) [30, 31]. As shown in Fig. 9, a Ag_3 aggregate is held together by the ^{t}BuC ≡ C group or CH_3O-(p-C_6H_4)-C ≡ C group and coordinated by three alternate pyridyl nitrogen atoms of the **Py[6]** ligand. The ^{1}H NMR spectra of **16** and **17** show two sets of well-resolved peaks for the coordinated and uncoordinated pyridine rings of **Py[6]** due to the excellent size match between **Py[6]** and the Ag_3 aggregate. It is noteworthy that such excellent size matching makes the Ag_3 aggregate to be the most favorable structure within **Py[6]** no matter what kind of and not affected by the external anions are introduced. In summary, the nuclearity number of metal cluster aggregates could be finely adjusted by altering the size of **Py[*n*]**s.

Taking advantage of the good ability of **Py[*n*]**s to stabilize reactive species and adjust the nuclearity number of silver clusters, it is envisioned that such fantastic protective effect of **Py[*n*]**s could facilitate the construction of metal cluster aggregates with higher nuclearity numbers and structural diversity by employing more complicated anion centers with di- or multiacetylide groups. For instance, a dumbbell-like structure containing two $[C \equiv CAg_3] \supset$ **Py[6]** moieties (**18**) is formed by using a 1,4-phenylenediacetylide dianion and **Py[6]** ligand. As shown in Fig. 10a, the two **Py[6]** macrocycles are in the arrangement of a parallel face-to-face geometry. Besides, the employment of 1,3-butadiynediide, which has a shorter linkage carbon chain between two acetylide groups, results in a C_4^{2-} bridged Ag_3-**Py[6]** unit (**19**) in a clam-like structure (Fig. 10b) [30]. Therein, the two **Py[6]** ligands in **19** shows an eclipsed face-to-face configuration with a dihedral angle of 23°. Further shortening the length of carbon linker leads to a fusion of the bridged $C \equiv CAg_3$ aggregates,

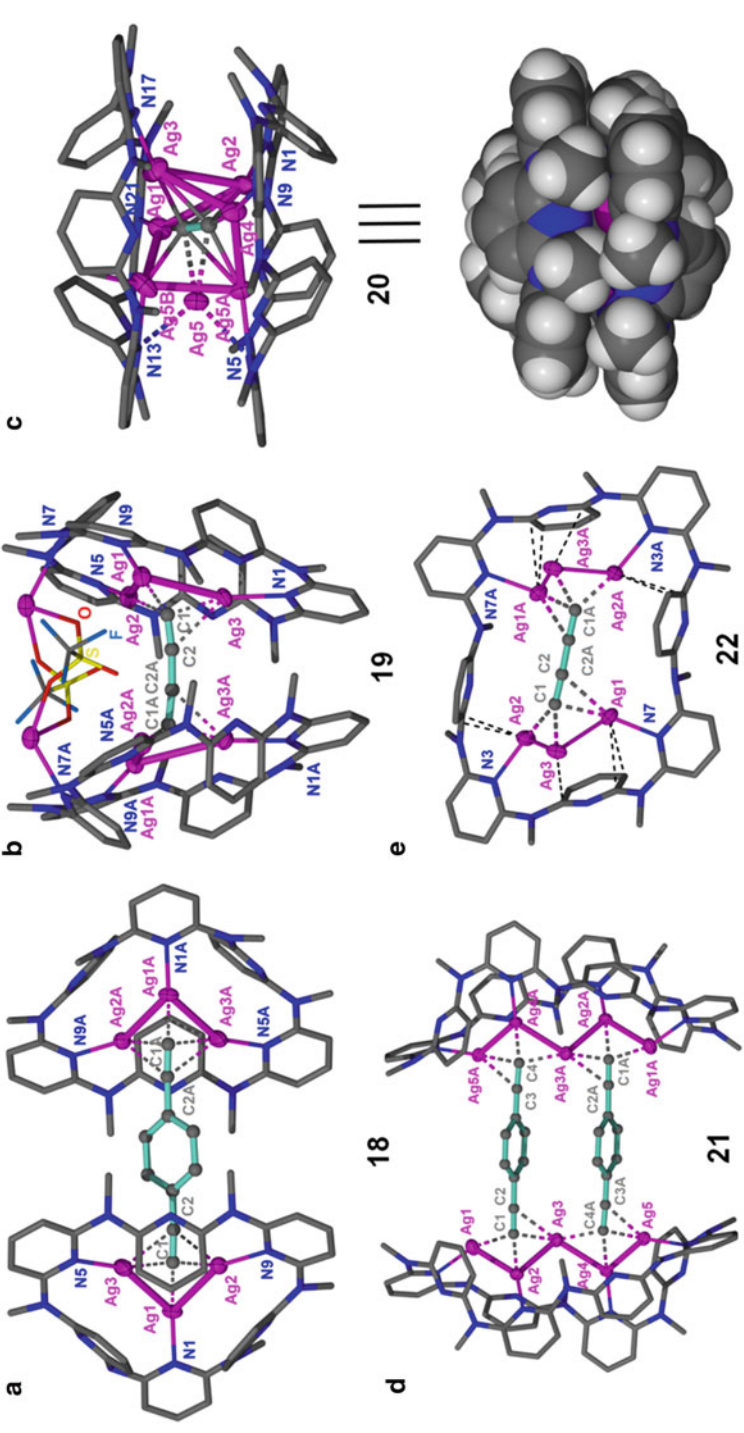

Fig. 10 Crystal structures of (**a**) $[Ag_6(C\equiv C\text{-}(p\text{-}C_6H_4)\text{-}C\equiv C)(\mathbf{Py[6]})_2](CF_3SO_3)_4{\cdot}2CH_2Cl_2$ (**18**), (**b**) $[(CF_3SO_3)_4Ag_8(C\equiv C\text{-}C\equiv C)(\mathbf{Py[6]})_2](CF_3SO_3)_2$ (**19**), (**c**) $\{[Ag_5(C\equiv C)(Py\text{-}[6])_2](CF_3SO_3)_3\}_{0.7}\{[Ag_6(C\equiv C)(\mathbf{Py\text{-}[6]})_2](CF_3SO_3)_4\}_{0.3}$ (**20**), (**d**) $[Ag_{10}\{1,4\text{-}(C\equiv C)_2C_6H_4\}_2(\mathbf{Py[8]})_2(CH_3OH)_2](BF_4)_6{\cdot}2H_2O$ (**21**), and (**e**) $[(CF_3SO_3)_4Ag_6(C\equiv C\text{-}C\equiv C)(\mathbf{Py[8]})(H_2O)_5]$ (**22**). Color coding: Ag, pink; N, blue; C, gray; O, red; the acetylide group is highlighted in green. (Reprinted with permission from [10]. Copyright 2018 American Chemical Society)

finally generating a C_2^{2-}-centered silver cage in **20** encircled between two **Py[6]** macrocycles (Fig. 10c) [30]. In this $C_2@Ag_{5-6}$ cluster, the silver aggregates are encapsulated by two parallel bowl-shaped **Py[6]** ligands that are associated together by multiple C-H···π and C-H···N interactions. A brief conclusion states that the relatively small **Py[6]** macrocycle tends to form an acetylide-centered Ag_3 aggregate and the length of linkage carbon chain between two acetylide groups would significantly affect the structure of metal cluster complexes. Thus, reactive and unstable metal cluster aggregates with structural diversity could be fabricated by using this macrocyclic template-directed strategy.

For **Py[8]** macrocycle with a larger cavity size, the study with these ditopic anion-centered silver cluster aggregates ($[1,4\text{-}(C \equiv C)_2C_6H_4]^{2-}$ and $[C \equiv C\text{-}C \equiv C]^{2-}$ in **18** and **19**) is carried out to gain further insights into the coordinative relationship between multitopic anions and differently sized **Py[*n*]**s. As shown in Fig. 10e, the employment of $[1,4\text{-}(C \equiv C)_2C_6H_4]^{2-}$ brings about the formation of $[Ag_3C \equiv C\text{-}C_6H_4\text{-}C \equiv CAg_3]$ aggregate, which is beyond the limit of **Py[8]**, thus leading to a fusion of two $[Ag_3C \equiv C\text{-}C_6H_4\text{-}C \equiv CAg_3]$ aggregates to a bigger $[Ag_5(C \equiv C\text{-}C_6H_4\text{-}C \equiv C)_2Ag_5]$ cluster in **21** with a zigzag-chain-like structure stabilized by two **Py[8]** macrocycles [32]. Besides, in contrast to the $C_2@Ag_{5-6}$ cluster stabilized by two **Py[6]**, a dumbbell-like $[Ag_3C \equiv C\text{-}C \equiv CAg_3]$ aggregate in **22** is encapsulated by one parallelogram-shaped **Py[8]**, resulting in a discrete cocoon-like structure (Fig. 10d). It is noteworthy that the larger macrocycle **Py[8]** is more flexible and could easily adapt to different cluster aggregates based on the extraordinary conformational tunability. Moreover, the nuclearity number and geometry of the encapsulated clusters would be finely adjusted by the anion center, shedding lights on the synthesis of a wide range of metal cluster aggregates.

For the **Py[*n*]**-based polyacetylide anion systems, some special metal cluster-centered metallosupramolecular architectures with high nuclearity number have been fabricated by altering the ring size. Taking the employment of the panel-like polyacetylide anion $[1,3,5\text{-}(C \equiv C)_3C_6H_3]^{3-}$ as an example, a series of metal cluster-centered metallocages are obtained based on differently sized **Py[*n*]** (n = 6–8) macrocycles (Fig. 11a) [33]. Structural studies reveal that the Ag_3-**Py[6]** unit is bonded to each acetylide moiety in the **Py[6]**-encircled complex **23**, and the resulting $[1,3,5\text{-}(Ag_3C \equiv C)_3C_6H_3]^{6+}$ aggregate is then encapsulated by three **Py[6]** macrocycles to achieve a trefoil geometry (Fig. 11b). The employment of a larger macrocycle **Py[7]** also gives rise to the same $[1,3,5\text{-}(Ag_3C \equiv C)_3C_6H_3]^{6+}$ species (Fig. 11c), but the three **Py[7]** ligands in complex **24** exhibit different conformations. ^{1}H NMR spectrum shows that the signals of proton of **Py[6]** in **23** are sharp and well-resolved. But for complex **24**, the mismatch between the large **Py[7]** and the relatively small Ag_3 aggregate results in very broad proton NMR signals of **Py[7]**. When an even larger macrocycle **Py[8]** is employed to the multitopic anionic system, two $[1,3,5\text{-}(Ag_3C \equiv C)_3C_6H_3]^{6+}$ aggregates fuse together to a Ag_5 aggregate as mentioned before, which is further encircled in the large cavity of **Py[8]** to form complex **25**. In this case, a triangular prism structure is generated based on three **Py[8]**-encapsulated Ag_5 clusters and two $[1,3,5\text{-}(C \equiv C)_3C_6H_3]$ units, which function as the pillars and panels, respectively (Fig. 11d). Moreover, as evidenced by

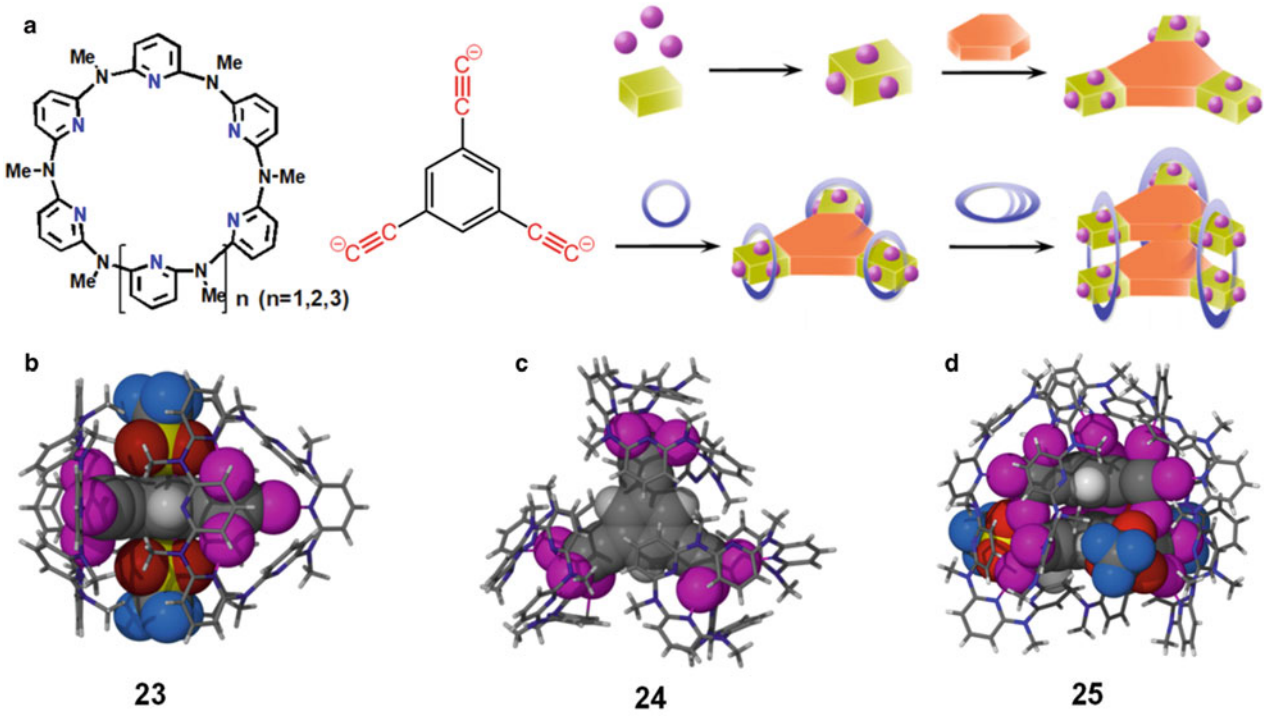

Fig. 11 (**a**) Scheme of the synthesis of metal cluster-centered metallocages with polyacetylide anion $[1,3,5\text{-}(C \equiv C)_3C_6H_3]^{3-}$ and differently sized **Py[*n*]** ($n = 6$–8) macrocycles. Crystal structures of (**b**) $[Ag_9\{1,3,5\text{-}(C \equiv C)_3C_6H_3\}(\mathbf{Py[6]})_3](CF_3SO_3)_6$ (**23**), (**c**) $[Ag_{20.5}\{1,3,5\text{-}(C \equiv C)_3C_6H_3\}_2(\mathbf{Py[7]})_6(CF_3SO_3)_4](CF_3SO_3)_{10.5}$ (**24**), and (**d**) $[Ag_{15}\{1,3,5\text{-}(C \equiv C)_3C_6H_3\}_2(\mathbf{Py[8]})_3(CF_3SO_3)_3](CF_3SO_3)_6$ (**25**). Color coding: Ag, pink; N, blue; C, gray; O, red. (Reprinted with permission from [10, 33]. Copyright 2018 American Chemical Society. Copyright 2012 Royal Society of Chemistry)

DOSY NMR spectrum and high-resolution ESI-MS, such complicated 3D structure shows fantastic stability and structural integrity in solution despite of the complex composition involving 3 **Py[8]** macrocycles, 15 silver atoms, 2 [1,3,5-(C ≡ C)$_3$C$_6$H$_3$] units, and triflate anions. Therefore, it is envisioned that macrocycle-based synthetic strategy is conducive to access a variety of metal cluster-centered polygonal and polyhedral architectures, which could enlarge the library of the extensively reported single-metal-based structures.

Ag_2S nanoclusters have attracted considerable attentions due to their intriguing near-infrared photoluminescent properties, semiconductor properties, and low toxicities to living tissues. However, it is still a challenge to prepare Ag_2S nanoclusters with tunable sizes under mild conditions. Inspired by the extraordinary property of size-tunable **Py[*n*]**s in the fabrication of polynuclear silver clusters of various acetylides, it is envisioned that such synthetic method could be applied to achieve the silver thiolate cluster precursors in a controllable manner, which would further facilitate the construction of desired Ag_2S nanoclusters. As shown in Fig. 12a, a typical-Ag_3 cluster aggregate **26** is established by using the **Py[6]** macrocycle [34]. X-ray diffraction studies present that such a Ag_3 aggregate is coordinated to the sulfur center through a μ_3-mode and is encapsulated by the **Py[6]** macrocycle via the coordination of three alternate pyridyl nitrogen atoms (Fig. 12a). The remaining three pyridine rings interact with the silver atoms based on the silver-aromatic π interactions. In contrast to previously reported μ_3 silver-thiolate cluster species, the Ag-S bond distances in **26** (2.339(3)–2.394(2) Å) are found to be shorter by 0.1–0.2 Å, indicating the strong size restriction effect of the peripheral coordinative **Py[6]** macrocycle. In another case, a Ag_5 cluster complex **27** is obtained based on a

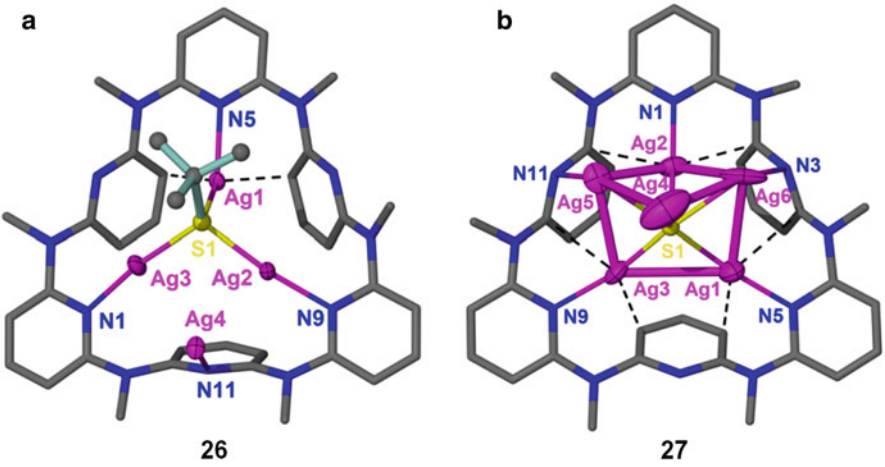

Fig. 12 Crystal structures of (**a**) [Ag_4(^{t}BuS)(CF_3SO_3)$_2$(**Py[6]**)](CF_3SO_3) (**26**) and (**b**) [Ag_5S(**Py[6]**)](CF_3SO_3)$_3$·CH_3OH (**27**). Color coding: Ag, pink; N, blue; C, gray; S, yellow; the acetylide group is highlighted in green. (Reprinted with permission from [10]. Copyright 2018 American Chemical Society)

single-atom dianion S^{2-} with three silver atoms coordinated by a bowl-shaped **Py[6]** macrocycle similar to that in complex **26** (Fig. 12b) [35]. Obviously, both the argentophilic interactions and silver-aromatic π interactions account for the stabilization of such a **Py[6]**-encircled Ag_5 cluster aggregates. Therefore, the size-tunable **Py[*n*]**s could be finely employed to access metal cluster aggregates with different kinds of external anion centers in a controllable way.

Further study involving a macrocycle **Py[7]** and halide anions has been carried out to investigate how the central anion variations within **Py[*n*]** macrocycles affect the structure of metal cluster aggregates [36]. As shown in Fig. 13a–c, the resulting silver halide clusters $[Ag_{3-4}X]$ (X = Cl, Br, I) all comprise a central halide-coordinated Ag_3 or Ag_4 aggregate inside **Py[7]** (complex **28**–**30**). Each silver atom bonded with the halide center is also supported by one or two nitrogen atoms of pyridine rings and further interact with the aromatic π systems (Ag-C distances, 2.515–2.705 Å). The Ag-Cl bond lengths in **28** are approximately 0.2 Å shorter than that in other reported pyramidal $[Ag_3Cl]$ clusters, and the chlorine atom is 0.34 Å above the Ag1-Ag2-Ag3 plane due to the restricted coordination of **Py[7]** (Fig. 13a). For a larger bromide center, the long Ag-Br lengths lead to an increased distance between the bromine atom and Ag_3 plane in **29** (Fig. 13b). Because of the small size of the $[Ag_3Cl]$ and $[Ag_3Br]$ clusters relative to the cavity size of **Py[7]**, one or two additional silver atoms are also included in the macrocyclic ligand. Moreover, the even larger atomic size of iodine leads to a longer Ag-I bond and an expanded Ag_3 triangle, resulting in the encapsulation of one more silver atom capping on the silver triangle. Thus, a trigonal bipyramidal $[IAg_4]$ cluster **30** is finally obtained with the iodide anion 0.92 Å above the Ag_3 plane (Fig. 13c). It is suggested by this study that the metal-anion bonding distances could be finely adjusted by the coordination restriction **Py[*n*]**s, which provides a potential method to access metal clusters with novel intrinsic properties.

Another new kind of neutral N-containing macrocyclic ligands has been developed to construct novel dicobalt amido complexes [37]. The geometric flexibility of the size-tunable macrocyclic ligands could easily adapt to various coordination environments of the metal ions by adjusting the number of catenated methylene units between imino nitrogen atoms. X-ray diffraction studies reveal that a chloride bridged dicobalt complex **31** is obtained with a folded structure by treatment of the ligand with $CoCl_2$, in which an acute angle of the macrocyclic plane is formed to satisfy the coordination environment of the dinuclear dicobalt complex (Fig. 14a). Substitution of the bridging chloride unit in **31** gives rise to the dark red azido complex **32** with a folded geometry similar to that of **31**. It is noteworthy that a pseudo-octahedral geometry is obtained for the Co^{II} ions in **32** (Fig. 14b), suggesting the lability of the coordinated phosphine moiety. Besides, the azido complex is stable under the addition of excess PR_3 (R = Me, Et), indicating that the PMe_3 ligation seems to be inert on **32**. Furthermore, when the azido complex **32** is heated with PMe_3, a diamagnetic amido complex **33** is formed in C_{2v} symmetry similar to that of complex **31** (Fig. 14c). ^1H NMR spectrum shows that the bridged amido NH_2 in **33** resonates at δ = 4.56 ppm. Moreover, a μ-phosphinimido dicobalt species **34** could also be fabricated by altering the number of catenated methylene units to an ethylene group in a similar synthetic method. Due to the relatively short linker, the macrocycle in **34** with weak flexibility displays a structure somewhere

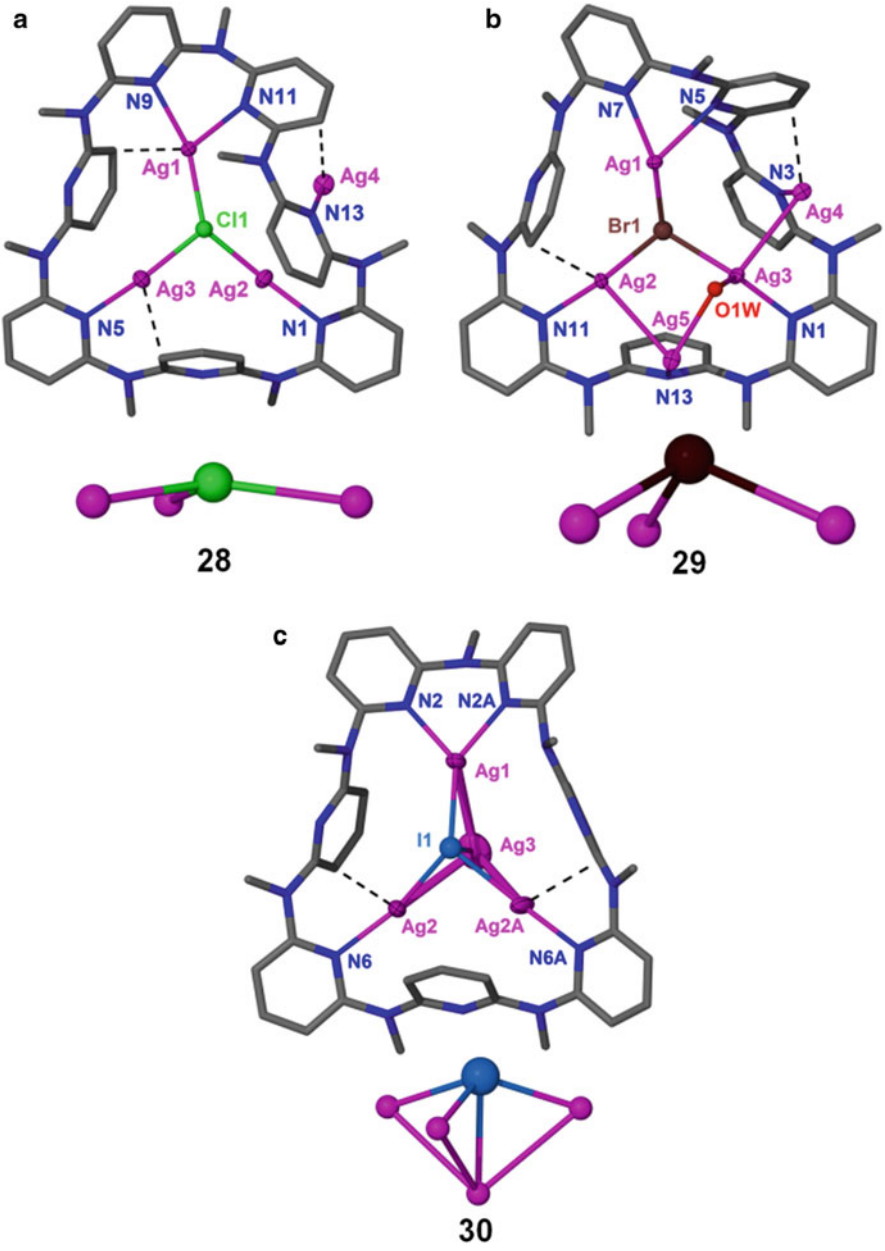

Fig. 13 Crystal structures of (**a**) $[Ag_4Cl(CF_3SO_3)_3(\mathbf{Py[7]})(CH_3OH)]$ (**28**), (**b**) $[Ag_5Br(CF_3SO_3)_2(H_2O)_4(\mathbf{Py[7]})](CF_3SO_3)_2{\cdot}H_2O$ (**29**), and (**c**) $[Ag_4I(H_2O)_2(\mathbf{Py[7]})](CF_3SO_3)_3$ (**30**). Color coding: Ag, pink; N, blue; C, gray; O, red; Cl, green; Br, brown; I, light blue. (Reprinted with permission from [10]. Copyright 2018 American Chemical Society)

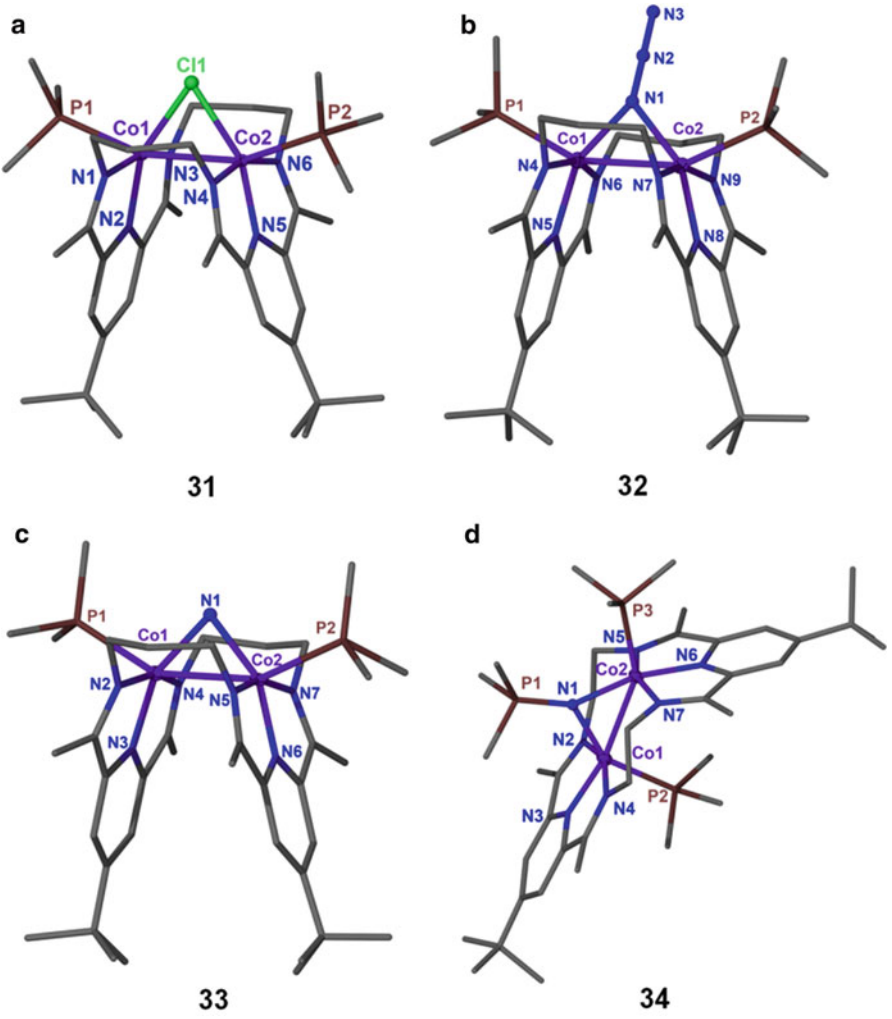

Fig. 14 Crystal structures of (**a**) [(^{3}PDI$_2$)Co$_2$(μ-Cl)-(PMe$_3$)$_2$][OTf]$_3$ (**31**), (**b**) [(^{3}PDI$_2$)Co$_2$(μ-N$_3$)(PMe$_3$)$_2$][OTf]$_3$ (**32**), (**c**) [(^{3}PDI$_2$)Co$_2$(μ-NH$_2$)(PMe$_3$)$_2$][OTf]$_3$ (**33**), and (**d**) [(^{2}PDI$_2$)Co$_2$(μ-NPMe$_3$)(PMe$_3$)$_2$][OTf]$_3$ (**34**) (PDI = 2,6-pyridyldiimine). Color coding: Co, purple; N, blue; C, gray; Cl, green; P, brown

in between the unfolded and folded geometries (Fig. 14d). The successful isolation of these structurally diversified dicobalt species suggests that both the ring size and reaction conditions would influence the product distributions, which could be applied to alter the Co$_2$(μ-N) core reactivity based on the reorganization abilities of differently sized macrocyclic ligands.

43.3 Applications of Metal Cluster-Macrocycle Adducts

43.3.1 Platform for Organometallic Transformations

In view of the abovementioned controllable synthesis of polynuclear metal clusters based on **Py[*n*]**s, the resulting metal-macrocycle capsules with high flexibility hold a great potential to conduct organometallic transformations for polymetalated heteroaromatic compounds. To date, many metal-ligand container architectures have been reported to encage guest molecules and stabilize highly reactive transition states of substrate molecules. Besides, a variety of reactions (e.g., Diels-Alder reaction [38], electrocyclization [39], and reductive elimination [40]) have been performed within organometallic capsules, and the resulting products show unusual selectivity and/or enhanced activity. However, the structurally well-defined reaction intermediates are rarely isolated due to the lack of flexible supramolecular coordination capsules with different cavity sizes.

Inspired by the remarkable dynamic feature of capsule-like **Py[8]**-Ag_3 cluster, which suggests an interconversion of various conformations of **Py[8]**-Ag_3 capsule at room temperature and a fixed rigid form at low temperatures, it is envisioned that such flexibility would allow this capsule to easily adapt to diverse polymetalated heteroaromatic compounds by organometallic transformations. For example, intramolecular an 5-*endo*-*dig* cyclization is observed to form a polymetalated indole complex 35 upon treatment of o-ethynylaniline with a solution of **Py[8]**-Ag_3 capsule and additional silver triflate [41]. The resulting dianionic indole ring in **35** is negatively charged at two vicinal carbon atoms and stabilized by a coplanar Ag_4 rectangle based on **Py[8]**. Notably, the structure of **35** features the first example of well-defined organosilver intermediate derived from Ag(I)-involved aminoalkyne cyclization transformations [42]. Additionally, the **Py[8]**-Ag_3 capsule-triggered cyclization can also be applied to other substrates containing both amine and ethynyl groups (Fig. 15), which experiences a new 6-*endo*-*dig* cyclization or cascade or multistep cyclization pathway triggered by the **Py[8]**-Ag_3 capsule to achieve the quinolinium, 2,2′-biindole, and benzo[*a*]carbazole architectures in **36**–**38**, respectively. Such macrocycle-based dynamic coordination capsule provides a feasible way to trigger cyclization reactions for various alkyne substrates under mild conditions. The isolation of these unprecedented structurally well-defined polysilver heteroaromatics and related theoretical studies deepen our understanding of multicentered bonding nature and metal-perturbed aromaticity in stabilization of the polysilver aromatic complexes, which could provide a probable way to develop more efficient and useful synthetic methods.

43.3.2 Stabilization of Intermediate Species

Copper-catalyzed oxidations have many significant applications in biological and synthetic systems. In view to get insights into the mechanisms of such oxidation catalysis, the synthesis and reactivity studies of various copper-oxygen intermediates have been widely carried out. Macrocycle-based copper systems have provided an

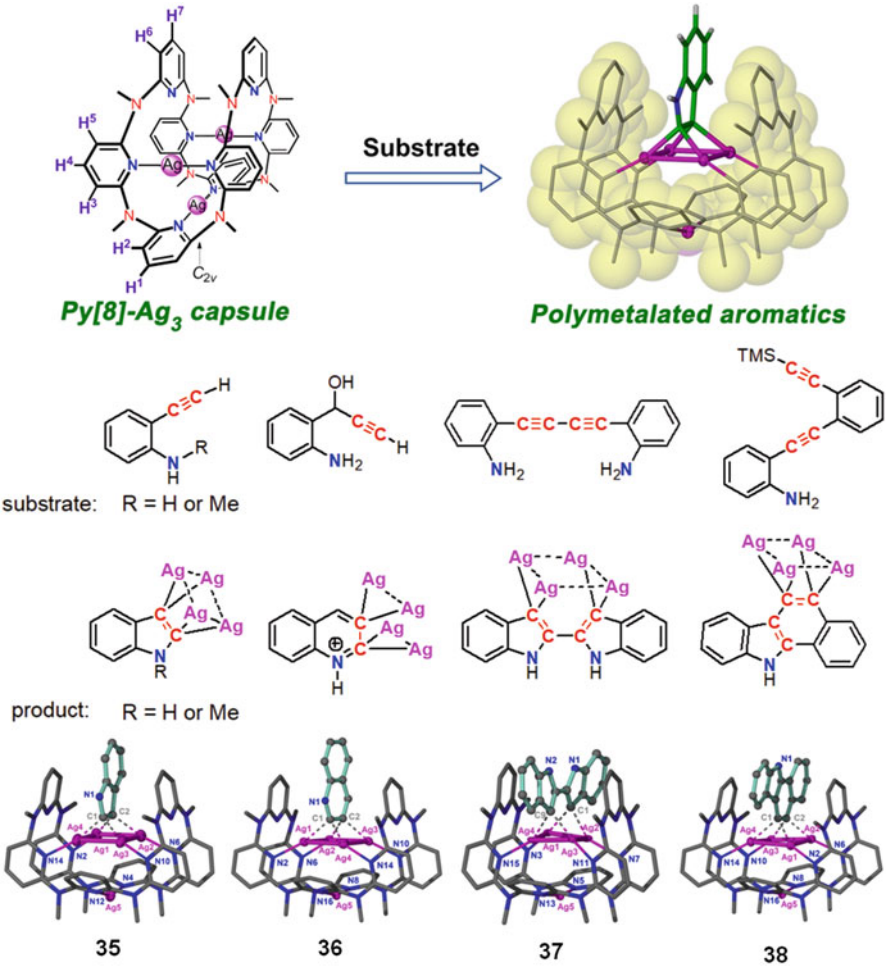

Fig. 15 Molecular structures of substrates and polysilver-bonded heteroaromatics formed within a **Py[8]**-Ag_3 capsule. Crystal structures of $[Ag_5(C_8NH_5)(\mathbf{Py[8]})](CF_3SO_3)_3$ (**35**), $[Ag_5(C_9NH_5)H(\mathbf{Py[8]})](CF_3SO_3)_4$ (**36**), $[Ag_5(C_{16}N_2H_{10})(\mathbf{Py[8]})](CF_3SO_3)_3$ (**37**), and $[Ag_5(C_{16}NH_9)(\mathbf{Py[8]})](CF_3SO_3)_3$) (**38**). Color coding: Ag, pink; N, blue; C, gray; O, red; the acetylide group is highlighted in green. (Reprinted with permission from [10, 41]. Copyright 2018 American Chemical Society. Copyright 2018 The Royal Society of Chemistry)

efficient tool to address this goal due to the extraordinary protective effect on reactive species. For example, a binuclear $[Cu^{II}(\mu\text{-OH})Na]$ species encircled by a macrocyclic ligand (complex **39**) has been found to stabilize the hydroxylation product of THF, resulting in a 2-hydroxytetrahydrofuran complex (THF-2-ol) protected by macrocycle in complex **40** [43].

X-ray crystal structure studies of **39** (Fig. 16a) reveal that the Cu^{II} ion is bonded to three neighboring N atoms on the macrocyclic ligand and is bridged by a hydroxyl

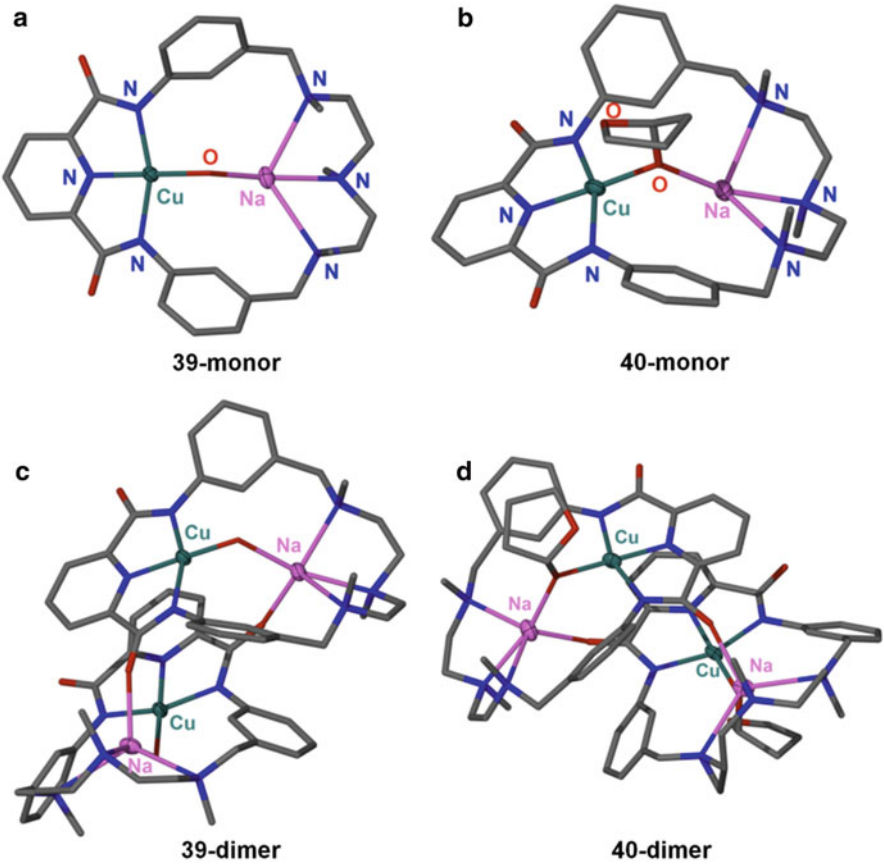

Fig. 16 Crystal structures of (**a**) the monor and (**c**) the dimer of [Cu^{II}(μ-OH)Na] species (**39**) and (**b**) the monor and (**d**) the dimer of [Cu^{II}(μ-O-THF)Na] species (**40**). Color coding: Cu, dark green; Na, light pink; N, blue; C, gray; O, red

group to a Na^{I} ion with a Cu···Na distance of 3.568(2) Å. It is intriguing that the complex crystallizes as a dimer as shown in Fig. 16c due to the interactions between the carboxamide carbonyl in one "monomer" and the Na^{+} ion in the other, resulting a five-coordinate Na^{I} ion in a distorted square-pyramidal geometry. Surprisingly, when complex **39** is treated with Cu^{I} in THF/CH_3CN in an attempt to substitute a Cu^{I} ion for the Na^{I} ion, only the deprotonated product of THF (complex **40**) is formed. X-ray crystal structure analysis shows that the THF-2-ol is bridged to the Cu^{II} and Na^{I} ions with a weak interaction between Cu^{II} and the O atom on THF (Fig. 16b, d). Isotope-labeling studies suggest that the oxygen atom in THF-2-ol is the source of the O atom in complex **39**. It is noteworthy that such hydroxylation of THF is not observed in THF solutions of Cu(III) with acyclic multidentate ligand, implying the unique role of such macrocycle-bonded metal systems in C-H activation process.

43.3.3 Macrocycle-Assisted Bulk-to-Cluster-to-Nanoparticle Transformations

On account of the coordination restriction of macrocyclic **Py[*n*]**s, the abovementioned silver cluster aggregates show unique metal-anion bond lengths and uncommon elemental ratios between the central anions and silver atoms. Therefore, it is envisioned that such distinctive metal cluster aggregates could be utilized as starting materials to access new functional compounds.

For example, the abovementioned **Py[7]**-based silver halide clusters $[Ag_{3–4}X]$ (X = Cl, Br, I) can be further transformed to nonstoichiometric silver halide nanoparticles $[Ag_mX_n]^{(m-n)+}$ (m > n; X = Cl, Br, I) by adding tetrafluoroboric acid to interrupt the coordination between the central silver aggregates and the surrounding **Py[7]** (Fig. 17a) [36]. The nonstoichiometric silver chloride nanoparticles are finally obtained after the protonation process together with the addition of the stabilizing surfactant polyvinylpyrrolidone (PVP). Moreover, the newly fabricated nonstoichiometric silver halide nanoparticles $[Ag_mX_n]^{(m-n)+}$ (m > n; X = Cl, Br, I) hold a great potential to act as an highly efficient electrocatalyst for the chlorine evolution reaction (CER), which is a fundamental and important electrochemical reaction in industry because of the extensive application of chlorine (e.g., in polymers and drugs). Besides, the nonstoichiometric elemental ratio between silver and halogen atoms results in the positively charged nature of the $[Ag_mX_n]^{(m-n)+}$ nanoparticles, which accelerates the transport process of chloride drived by electrostatic attraction and thus facilitates the formation of the catalytically active silver polychloride species. Such enhanced catalytic efficiency also results from the formation of uncommon nonstoichiometric nanoparticles, which makes the coordinatively unsaturated silver active sites easily access to catalyze the chloride oxidation (Fig. 17b). In this regard, the involvement of the $[Ag_mX_n]^{(m-n)+}$ nanoparticles could provide an efficient tool to catalyze the CER at a very low overpotential. In addition, the positively charged surface of the nonstoichiometric $[Ag_mX_n]^{(m-n)+}$ nanoparticles makes it attract chloride anions more easily than neutral water molecules, leading to a high selectivity for the CER over the oxygen evolution reaction (Fig. 17c).

Given that silver sulfide has long been investigated as a type of narrow bandgap semiconductor owing to its good stability, low toxicity, and widespread potential applications in photovoltaic cells, photoconductors, and near-infrared imaging [44], the construction of diversiform silver sulfide species has attracted tremendous research interests. Besides a bandgap of 0.9–1.1 eV for bulk α-Ag_2S [45], the synthesis of nano-sized Ag_2S provides an efficient method to finely enlarge the bandgap based on the quantum confinement effect, which brings about many fantastic size-specific optical and optoelectronic properties [46]. Therefore, it is necessary to develop an effective method to access uniformly sized Ag_2S nanocrystals. However, among the previously explored methods (e.g., the microemulsion approach [47] and the hot injection method [48]), the use of exotic ligand- or surfactant-stabilized silver and sulfide ions or their precursors as well as the requirement of elevated temperature and high pressure in most cases impedes the synthesis of uniformly sized Ag_2S nanocrystals [49]. Thus, an alternative method that direct transform bulk Ag_2S

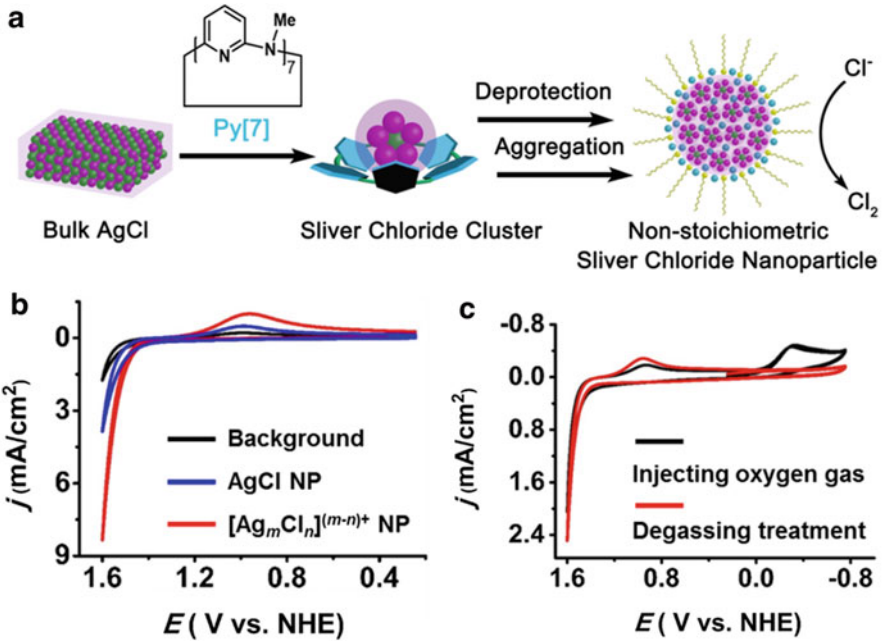

Fig. 17 (**a**) Scheme for the formation of nonstoichiometric silver halide nanoparticles as CER reaction electrocatalysts. (**b**) Cyclic voltammograms (CVs) at a glassy carbon electrode in an aqueous solution of NaCl (1 M). (**c**) CVs at a glassy carbon electrode in an aqueous solution of NaCl with the nonstoichiometric $[Ag_mCl_n]^{(m-n)+}$ nanoparticle ($c_{Ag^+} = 0.53$ μM) as a catalyst after degassing (red) or after bubbling oxygen (black). (Reprinted with permission from [10, 36]. Copyright 2018 American Chemical Society. Copyright 2017 The Royal Society of Chemistry)

solid into its nano-sized prototype would be a convenient and ideal synthetic strategy. In this case, the abovementioned macrocycle-assisted bulk-to-cluster-to-nanoparticle transformation could also be applied to the silver sulfide systems.

Taking into consideration that the $[Ag_5S]$-containing complex **27** could be stabilized by macrocyclic **Py[6]**, this macrocyclic ligand is thus utilized to produce two new precursor clusters **41** and **42** by varying its amount [35]. As shown in Fig. 18b, a dumbbell-shaped $[Ag_{12}S_2]$ silver sulfide cluster aggregate is found to be embraced by two macrocyclic **Py[6]**s at the upper and nether sides in complex **41**. For complex **42**, the $[Ag_5S]$ cluster aggregate is protected by two face-to-face **Py[6]** macrocycles (Fig. 18c). It is worth noting that the Ag-S bond lengths in **41 and 42** are ~0.2 Å shorter than that in bulk Ag_2S due to the coordination restriction of **Py[6]** [50]. In view of the fact that the single $[Ag_5S]$ and joint $[Ag_{12}S_2]$ silver sulfide clusters can be successfully isolated by varying the amount of protective **Py[6]**, the coalescence and fusion of **Py[6]**-encapsulated $[Ag_5S]$ clusters are suggested as a promising tool to access nonstoichiometric Ag-S binary nanoparticles.

For the bulk-to-cluster-to-nanoparticle transformation of Ag_2S (Fig. 18a), protonation of these macrocycle-encircled complexes results in the release of the deprotected silver sulfide clusters, which will further undergo the formation of silver sulfide nanoparticles. Further characterization by energy-dispersive

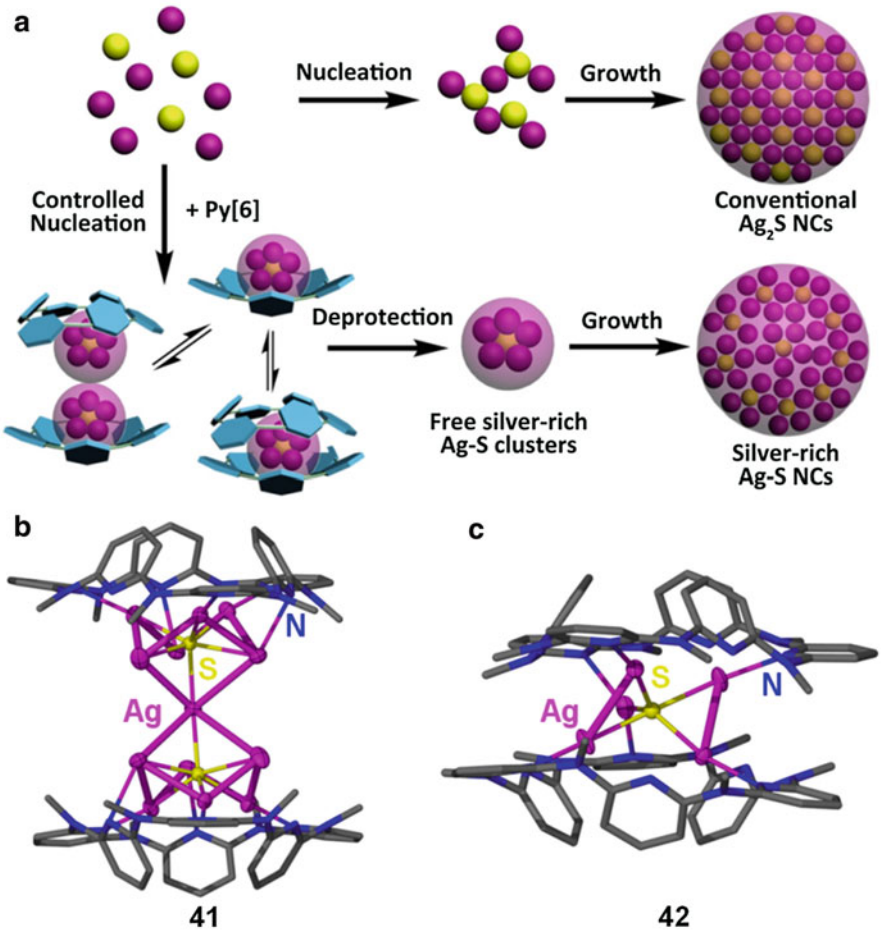

Fig. 18 (**a**) Schematic diagram for the bulk-to-cluster-to-nanoparticle transformation of **Py[6]**-protected Ag_2S species. (**b**) Crystal structures of $[Ag_{12}S_2(\mathbf{Py[6]})_2](CF_3SO_3)_8{\cdot}H_2O{\cdot}CH_3OH$ (**41**) and $[Ag_5S(\mathbf{Py[6]})_2](CF_3SO_3)_3$ (**42**). Color coding: Ag, pink; N, blue; C, gray; S, yellow

X-ray measurements reveals the existence of Ag and S and further offers the Ag/S atomic ratio of 3.5. Additionally, X-ray photoelectron spectroscopy suggests a + 1 oxidation state of the silver atoms in the nanoparticles, and the Ag/S molar ratio is determined to be 3.7, which is comparable to the energy dispersive X-ray spectroscopy result of 3.5 and larger than the values of around 2.0 in bulk Ag_2S [47]. It is conjectured that such a high Ag/S ratio is actually resulted from the **Py[6]**-encapsulated silver-rich Ag-S clusters. The bandgap energy of the nanoparticle with a high Ag/S ratio is thus deduced to be 4.0 eV, leading to a large blueshift relative to that of bulk α-Ag_2S. Theoretical calculation for HOMO-LUMO gap of silver sulfide clusters with different Ag/S ratios is carried out to clarify the relationship between the energy gap and the Ag/S ratio in silver sulfide clusters. DFT calculations show that the cluster with a higher Ag/S ratio

has more localized HOMO-LUMO orbital and a larger energy gaps correspondingly. On account of such advantages mentioned above, this new synthetic method provides a viable tool to tune the bandgap of binary nanomaterials by different element ratios instead of the size. Aside from this, the present macrocycle-assisted bulk-to-cluster-to-nanoparticle transformation is also applicable to the efficient synthesis of alkynyl-protected silver nanoclusters and thiolate-protected Ag_2S nanoclusters.

43.4 Conclusions and Perspectives

This chapter highlights the employment of polydentate macrocycles as an outer template to direct the construction of various polynuclear metal clusters in a controllable manner. Clearly, the intrinsic macrocyclic effect and the cooperative coordination effect of macrocyclic ligand systems contribute to their superiority in metal cluster assemblies. In particular, neutral polydentate macrocycles have shown good behaviors in the assembly of metal cluster aggregates containing various externally introduced anions, which provide an efficient method to achieve structurally diversified metal cluster aggregates. Preliminary application studies of the macrocycle-encapsulated metal clusters have also been described, such as the uncommon organometallic transformations and a **Py[*n*]**-assisted bulk-to-cluster-to-nanoparticle transformation that can be used to fabricate novel nanomaterials with unique physical and catalytic properties.

It is envisioned that many other symmetric or unsymmetric macrocycles could be elaborately designed and synthesized as templates to direct the synthesis of metal clusters with homo- or heteronuclear metal atoms in a controllable way. In this way, the macrocycle-protected metal clusters with structural diversity would provide an ideal molecular platform to study the structure-property relationship of metal clusters in view of their satisfying stability.

43.5 Cross-References

► Emerging Macrocyclic Arenes Related to Calixarenes and Pillararenes
► Stimuli-Responsive Self-Assembly Based on Macrocyclic Hosts and Biomedical Applications

Acknowledgments Financial support by the National Natural Science Foundation of China is gratefully acknowledged.

References

1. Sono M, Roach MP, Coulter ED, Dawson JH (1996) Heme-containing oxygenases. Chem Rev 96:2841–2887
2. Brown KL (2005) Chemistry and enzymology of vitamin B_{12}. Chem Rev 105:2075–2149

3. Ogoshi T, Yamagishi T, Nakamoto Y (2016) Pillar-shaped macrocyclic hosts pillar[n]arenes: new key players for supramolecular chemistry. Chem Rev 116:7937–8002
4. Kim DS, Sessler JL (2015) Calix[4]pyrroles: versatile molecular containers with ion transport, recognition, and molecular switching functions. Chem Soc Rev 44:532–546
5. Xue M, Yang Y, Chi X, Zhang Z, Huang F (2012) Pillararenes, a new class of macrocycles for supramolecular chemistry. Acc Chem Res 45:1294–1308
6. Frischmann PD, MacLachlan MJ (2008) Schiff base macrocycles reliable templates for multinuclear metallocavitands. Comments Inorg Chem 29:26–45
7. Park S-H, Lee S-Y, Park K-M, Lee S-S (2012) Supramolecular networking of macrocycles based on exo-coordination: from discrete to continuous frameworks. Acc Chem Res 45:391–403
8. Galana A, Ballester P (2016) Stabilization of reactive species by supramolecular encapsulation. Chem Soc Rev 45:1720–1737
9. Gloe K (2005) Macrocyclic chemistry: current trends and future perspectives. Springer, Dordrecht, and references therein
10. Zhang S, Zhao L (2018) Macrocycle-encircled polynuclear metal clusters: controllable synthesis, reactivity studies, and applications. Acc Chem Res 51:2535–2545
11. Kobayashi M, Shimizu S (1998) Metalloenzyme nitrile hydratase: structure, regulation, and application to biotechnology. Nature Biotech 16:733–736
12. Butler A, Sandy M (2009) Mechanistic considerations of halogenating enzymes. Nature 460:848–854
13. Hu Y, Ribbe MW (2016) Biosynthesis of the metalloclusters of nitrogenases. Annu Rev Biochem 85:455–483
14. Wang VC-C, Maji S, Chen PP-Y, Lee HK, Yu SS-F, Chan SI (2017) Alkane oxidation: methane monooxygenases, related enzymes, and their biomimetics. Chem Rev 117:8574–8621
15. Machonkin TE, Quintanar L, Palmer AE, Hassett R, Severance S, Kosman DJ, Solomon EI (2011) Spectroscopy and reactivity of the type 1 copper site in Fet3p from *saccharomyces cerevisiae*: correlation of structure with reactivity in the multicopper oxidases. J Am Chem Soc 123:5507–5517
16. Lieberman RL, Rosenzweig AC (2005) Crystal structure of a membrane-bound metalloenzyme that catalyses the biological oxidation of methane. Nature 434:177–182
17. Ogoshi T, Yamagishi T, Nakamoto Y (2016) Pillar-shaped macrocyclic hosts pillar[n]arenes: new key players for supramolecular chemistry. Chem Rev 116:7937–8002
18. Kim DS, Sessler JL (2015) Calix[4]pyrroles: versatile molecular containers with ion transport, recognition, and molecular switching functions. Chem Soc Rev 44:532–546
19. Zhang M, Yan X, Huang F, Niu Z, Gibson HW (2014) Stimuli-responsive host-guest systems based on the recognition of cryptands by organic guests. Acc Chem Res 47:1995–2005
20. Kulatilleke CP (2007) Characterization and properties of the copper(II/I) complexes of macrocyclic hexathiaether ligand [21]aneS_6. Polyhedron 26:1166–1172
21. Shaw JL, Wolowska J, Collison D, Howard JAK, McInnes EJL, McMaster J, Blake AJ, Wilson C, Schröder M (2006) Redox non-innocence of thioether macrocycles: elucidation of the electronic structures of mononuclear complexes of gold(II) and silver(II). J Am Chem Soc 128:13827–13839
22. Habata Y, Seo J, Otawa S, Osaka F, Noto K, Lee SS (2006) Synthesis of diazahexathia-24-crown-8 derivatives and structures of Ag^+ complexes. Dalton Trans 18:2202–2206
23. Helm ML, Hill LL, Lee JP, van Derveer DG, Grant GJ (2006) Cadmium-113 NMR studies on homoleptic complexes containing thioether ligands: the crystal structures of [Cd([12]aneS_4)$_2$](ClO_4)$_2$, [Cd([18]aneS_4N_2)](PF_6)$_2$ and [Cd([9]aneS_3)$_2$](PF_6)$_2$. Dalton Trans 29:3534–3543
24. Newell M, Ingram JD, Easun TL, Vickers SJ, Adams H, Ward MD, Thomas JA (2006) Structure and properties of dinuclear [Ru^{II}([n]aneS_4)] complexes of 3,6-Bis(2-pyridyl)-1,2,4,5-tetrazine. Inorg Chem 45:821–827
25. Frischmann PD, Gallant AJ, Chong JH, MacLachlan MJ (2008) Zinc carboxylate cluster formation in conjugated metallomacrocycles: evidence for templation. Inorg Chem 47:101–112
26. Frischmann PD, MacLachlan MJ (2007) Capsule formation in novel cadmium cluster metallocavitands. Chem Commun 43:4480–4482

27. Yamashita A, Watanabe A, Akine S, Nabeshima T, Nakano M, Yamamura T, Kajiwara T (2011) Wheel-shaped $Er^{III}Zn^{II}_3$ single-molecule magnet: a macrocyclic approach to designing magnetic anisotropy. Angew Chem Int Ed 50:4016–4019
28. Wang M-X (2012) Nitrogen and oxygen bridged calixaromatics: synthesis, structure, functionalization, and molecular recognition. Acc Chem Res 45:182–195
29. Gao C-Y, Zhao L, Wang M-X (2011) Designed synthesis of metal cluster-centered pseudorotaxane supramolecular architectures. J Am Chem Soc 133:8448–8451
30. Gao C-Y, Zhao L, Wang M-X (2012) Stabilization of a reactive polynuclear silver carbide cluster through the encapsulation within a supramolecular cage. J Am Chem Soc 134:824–827
31. Guo H, He X, Wan C-Q, Zhao L (2016) A stepwise bulk-to-cluster-to-particle transformation toward the efficient synthesis of alkynyl-protected silver nanoclusters. Chem Commun 52:7723–7726
32. Gao C-Y, He X, Zhao L, Wang M-X (2012) Dual template synthesis of silver acetylide cluster-encapsulated supramolecular boxes. Chem Commun 48:8368–8370
33. He X, Gao C-Y, Wang M-X, Zhao L (2012) Designed synthesis of a metal cluster-pillared coordination cage. Chem Commun 48:10877–10879
34. Chen H-Q, He X, Guo H, Fu N-Y, Zhao L (2015) Designed synthesis of size-tunable Ag_2S nanoclusters via distinguishable C-S bond cleavage reaction of alkyl- and aryl-thiolates. Dalton Trans 44:3963–3966
35. He X, Wang Y, Gao C-Y, Jiang H, Zhao L (2015) A macrocycle-assisted nanoparticlization process for bulk Ag_2S. Chem Sci 6:654–658
36. Zhang Q-Y, He X, Zhao L (2017) Macrocycle-assisted synthesis of non-stoichiometric silver(I) halide electrocatalysts for efficient chlorine evolution reaction. Chem Sci 8:5662–5668
37. Cui P, Wang Q, McCollom SP, Manor BC, Carroll PJ, Tomson NC (2017) Ring-size-modulated reactivity of putative dicobalt-bridging nitrides: C@H activation versus phosphinimide formation. Angew Chem Int Ed 56:15979–15983
38. Inokuma Y, Yoshioka S, Fujita M (2010) A molecular capsule network: guest encapsulation and control of Diels-Alder reactivity. Angew Chem Int Ed 49:8912–8914
39. Hastings CJ, Pluth MD, Bergman RG, Raymond KN (2010) Enzyme-like catalysis of the nazarov cyclization by supramolecular encapsulation. J Am Chem Soc 132:6938–6940
40. Kaphan DM, Levin MD, Bergman RG, Raymond KN, Toste FD (2015) A supramolecular microenvironment strategy for transition metal catalysis. Science 350:1235–1238
41. He X, Xue Y, Li C-C, Wang Y, Jiang H, Zhao L (2018) Synthesis of stable polymetalated aromatic complexes through metal-macrocycle capsule-triggered cyclization. Chem Sci 9:1481–1487
42. van Esseveldt BCJ, van Delft FL, Smits JMM, de Gelder R, Schoemaker HE, Rutjesa FPJT (2004) Transition metal-catalyzed synthesis of novel biologically relevant tryptophan analogues. Adv Synth Catal 346:823–834
43. Halvagar MR, Tolman WB (2013) Isolation of a 2-hydroxytetrahydrofuran complex from copper promoted hydroxylation of THF. Inorg Chem 52:8306–8308
44. Sadovnikov SI, Gusev AI (2017) Recent progress in nanostructured silver sulfide: from synthesis and nonstoichiometry to properties. J Mater Chem A 5:17676–17704
45. Kershaw SV, Susha AS, Rogach AL (2013) Narrow bandgap colloidal metal chalcogenide quantum dots: synthetic methods, heterostructures, assemblies, electronic and infrared optical properties. Chem Soc Rev 42:3033–3087
46. Wang RY, Tangirala R, Raoux S, Jordan-Sweet JL, Milliron DJ (2012) Ionic and electronic transport in Ag_2S nanocrystal-GeS_2 matrix composites with size-controlled Ag_2S nanocrystals. Adv Mater 24:99–103
47. Jiang X, Xie Y, Lu J, Zhu L, He W, Qian Y (2001) In-situ interface self-assemblies of nanocrystalline Ag_2E (E = S, Se, or Te) via chalcogen directional transfer agents. J Mater Chem 11:584–588

48. Wang D, Xie T, Peng Q, Li Y (2008) Ag, Ag_2S, and Ag_2Se nanocrystals: synthesis, assembly, and construction of mesoporous structures. J Am Chem Soc 130:4016–4022
49. Kershaw SV, Susha AS, Rogach AL (2013) Narrow bandgap colloidal metal chalcogenide quantum dots: synthetic methods, heterostructures, assemblies, electronic and infrared optical properties. Chem Soc Rev 42:3033–3087
50. Santamaría-Perez D, Marqués M, Chuliá-Jordán R, Menendez JM, Gomis O, Ruiz-Fuertes J, Sans JA, Errandonea D, Recio JM (2012) Compression of silver sulfide: X-ray diffraction measurements and total-energy calculations. Inorg Chem 51:5289–5298